Rat airway smooth muscle cell during actin modulation: rheology and glassy dynamics

Rachel E. Laudadio, Emil J. Millet, Ben Fabry, Steven S. An, James P. Butler and Jeffrey J. Fredberg

Am J Physiol Cell Physiol 289:1388-1395, 2005. First published Aug 24, 2005;
doi:10.1152/ajpcell.00060.2005

AJP - Cell Physiology is dedicated to innovative approaches to the study of cell and molecular physiology. It is published 12 times a year (monthly) by the American Physiological Society, 9650 Rockville Pike, Bethesda MD 20814-3991. ISSN: 0363-6143, ESSN: 1522-1563. Visit our website at http://www.the-aps.org/.

Am J Physiol Cell Physiol 289: C1388–C1395, 2005.
First published August 17, 2005; doi:10.1152/ajpcell.00060.2005.

Rat airway smooth muscle cell during actin modulation: rheology and glassy dynamics

Rachel E. Laudadio,[1] Emil J. Millet,[1] Ben Fabry,[2] Steven S. An,[1] James P. Butler,[1] and Jeffrey J. Fredberg[1]

[1]*Physiology Program, Department of Environmental Health, Harvard School of Public Health, Boston, Massachusetts; and* [2]*Physics Department, Erlangen University, Erlangen, Germany*

Submitted 11 February 2005; accepted in final form 9 July 2005

Laudadio, Rachel E., Emil J. Millet, Ben Fabry, Steven S. An, James P. Butler, and Jeffrey J. Fredberg. Rat airway smooth muscle cell during actin modulation: rheology and glassy dynamics. *Am J Physiol Cell Physiol* 289: C1388–C1395, 2005. First published August 17, 2005; doi:10.1152/ajpcell.00060.2005.—Although changes of cytoskeleton (CSK) stiffness and friction can be induced by diverse interventions, all mechanical changes reported to date can be scaled onto master relationships that appear to be universal. To assess the limits of the applicability of those master relationships, we focused in the present study on actin and used a panel of actin-manipulating drugs that is much wider than any used previously. We focused on the cultured rat airway smooth muscle (ASM) cell as a model system. Cells were treated with agents that directly modulate the polymerization (jasplakinolide, cytochalasin D, and latrunculin A), branching (genistein), and cross linking (phallacidin and phalloidin oleate) of the actin lattice. Contractile (serotonin, 5-HT) and relaxing (dibutyryl adenosine 3′,5′-cyclic monophosphate, DBcAMP) agonists and a myosin inhibitor (ML-7) were also tested for comparison, because these agents may change the structure of actin indirectly. Using optical magnetic twisting cytometry, we measured elastic and frictional moduli before and after treatment with each agent. Stiffness increased with frequency as a weak power law, and changes of friction paralleled those of stiffness until they approached a Newtonian viscous limit. Despite large differences in the mechanism of action among the interventions, all data collapsed onto master curves that depended on a single parameter. In the context of soft glassy systems, that parameter would correspond to an effective temperature of the cytoskeletal matrix and reflect the effects of molecular crowding and associated molecular trapping. These master relationships demonstrate that when the mechanical properties of the cell change, they are constrained to do so along a special trajectory. Because mechanical characteristics of the cell shadow underlying molecular events, these results imply special constraints on the protein-protein interactions that dominate CSK mechanical properties.

structural damping; scale-free; glass

RECENTLY, WE REPORTED a striking analogy in which the cytoskeleton (CSK) of the adherent cell was demonstrated to adjust its mechanical properties and modulate its malleability in much the same way as a glassblower fashions a work of glass (5, 14, 15, 36). Instead of changing temperature, however, the cell changes a temperature-like property that has much the same effect.

The hypothesis that the CSK might behave similarly to a glassy material was first suggested by Fabry et al. (14, 15), who measured stiffness and friction in a variety of cell types in culture, including the human airway smooth muscle (ASM) cell. Their report contained two surprising results. They had set out to identify distinct internal time scales (i.e., molecular relaxation times or time constants) that might reflect molecular dynamics of proteins integrated within the cytoskeletal lattice, and in particular they had expected to find relaxation time scales corresponding to myosin-actin cycling rates. Surprisingly, across a spectrum spanning five decades of frequency, f, and in all five of the cell types that were investigated, they found no characteristic time scales; rather, stiffness increased as f^{x-1}, implying that relaxation times were distributed as a power law, with a great many relaxation processes contributing when the frequency of the imposed deformation was small but fewer contributing as the frequency was increased and slower processes became progressively frozen out of the response. Thus no distinct internal time scale could typify protein-protein interactions; all time scales were present simultaneously but were distributed broadly. Because no distinct time scales characterize the response, behavior of this kind is referred to as being scale-free. Using other techniques and differing cell types, other researchers have confirmed that cytoskeletal dynamics are scale-free (1, 3, 8, 25, 32).

The second surprise was an unexpected relationship between changes in cell mechanics that arise when cytoskeleton constituents are modulated. In the living cell, the rheology of the CSK matrix is influenced by many structural proteins and their interactions. Despite this complexity, if stiffness or friction data were appropriately scaled and then plotted against x (which is readily determined from the power law exponent of stiffness vs. frequency), all data collapsed onto the same relationship regardless of the cell type studied, the signal transduction pathway activated, or the particular molecule manipulated (13, 14).

Purely as a matter of phenomenology, the observations described above firmly establish that the parameter x determines where the CSK sits along a continuous spectrum of solidlike vs. fluidlike states (15). In the limit in which x approaches 1, the behavior approaches that of a Hookean elastic solid and, in the limit in which x approaches 2, the behavior approaches that of a Newtonian viscous fluid. Values of x for adherent living cells fall in the range of 1.1–1.3, placing them closer to the solidlike than to the fluidlike state. Moreover, the parameter x was subsequently found to bring together into one phenomenological picture not only cytoskeletal stiffness and friction but also remodeling (5, 36).

Address for reprint requests and other correspondence: J. J. Fredberg, Harvard School of Public Health, Bldg. 1, Rm. 317, 665 Huntington Ave., Boston, MA 02115-6021 (e-mail: jfredber@hsph.harvard.edu).

The costs of publication of this article were defrayed in part by the payment of page charges. The article must therefore be hereby marked "*advertisement*" in accordance with 18 U.S.C. Section 1734 solely to indicate this fact.

With regard to mechanism of action, classical theories of viscoelasticity and equilibrium systems fail to account for these observations (5), and the physical significance of the parameter x remains elusive. Our working hypothesis holds that the CSK behaves as a glassy system and that the parameter x, which is easily measured, corresponds to an effective temperature of the CSK lattice (5, 13, 14, 36). In that case, the system is regarded as being frozen when x is close to 1 and melted when x is close to 2. Although the underlying physics remain poorly understood, strong experimental support for x as an effective temperature of the cytoskeletal lattice has recently been reported (5, 36).

Master relationships reported to date were obtained using only a small panel of experimental interventions, however, and used only one agent targeted specifically at actin (cytochalasin D). In the present study, we targeted actin using a range of interventions that was substantially wider than any studied previously. We show that these data confirm and substantially extend previous reports. We conclude by speculating about mechanisms that might account for the ability of an effective temperature to unify these observations.

MATERIALS AND METHODS

Cell isolation and culture. Rat tracheal smooth muscle cells were isolated and cultured as previously described by An et al. (2). Cells were grown to confluence in culture flasks placed into a 37°C humidified incubator containing 5% CO_2. Fresh DMEM-Ham's F-12 medium supplemented with streptomycin, penicillin, amphotericin B, and 10% FBS was added every 2–3 days. Cells were passaged with a solution containing 0.25% trypsin and 0.02% EDTA.

Materials. DMEM-Ham's F-12 medium, Fungizone, and 0.02% trypsin were purchased from GIBCO (Gaithersburg, MD). PBS was obtained from BioWhittaker (Walkersville, MD). Other reagents for tissue culture were ordered from Sigma (St. Louis, MO). Synthetic arginine-glycine-aspartic acid (RGD)-containing peptide (Peptite 2000) was obtained from Integra Life Sciences (San Diego, CA). Collagen I was procured from Cohesion (Palo Alto, CA). Drugs were acquired from Sigma, Calbiochem (La Jolla, CA), or Tocris Cookson (Ellisville, MO). They were reconstituted in sterile water [serotonin, dibutyryl adenosine 3′,5′-cyclic monophosphate (DBcAMP)], DMSO [cytochalasin D, latrunculin A, 1-(5-iodonaphthalene-1-sulfonyl)-1H-hexahydro-1,4-diazepine (ML-7), genistein, phalloidin oleate, and jasplakinolide], or methanol (phallacidin). Controls for the solvents were shown previously to have no effect on cellular mechanics (2).

The panel of agents and the concentrations used, as well as the presumed mechanisms of action, are summarized in Table 1. In separate experiments, we determined the incubation time for each agent to cause its maximum effect. Latrunculin A and cytochalasin D result in net actin depolymerization by binding to monomeric actin (G-actin) and capping filamentous actin (F-actin), respectively (27). Phalloidin is an actin-stabilizing peptide. Phallacidin and phalloidin oleate are two membrane-permeable phalloidin analogs (33). Jasplakinolide results in net actin polymerization by promoting both linear and branched growth of actin fibers (26). Genistein is a nonspecific blocker of tyrosine kinases (6). These kinases are necessary for the phosphorylation of the complex of actin-binding proteins at the branch sites of actin fibers.

For comparison with drugs that act directly on actin, we also used three drugs that work mainly through myosin: 5-HT, which increases internal Ca^{2+} and activates myosin light-chain kinase (MLCK) (35); DBcAMP, which decreases internal Ca^{2+} and activates myosin light-chain phosphatase (MLCP) (43); and 1-(5-iodonaphthalene-1-sulfonyl)-1H-hexahydro-1,4-diazepine (ML-7), which is a MLCK inhibitor (30).

Table 1. *Drug interventions*

Drug	Concentration, μM	Main Effect
5-HT	10.0	Contractile agonist, ↑ $[Ca^{2+}]_i$, activate MLCK
Cytochalasin D	2.0	Caps the actin filament, net depolymerization
DBcAMP	1,000	Relaxing agonist, ↓ $[Ca^{2+}]_i$, activate MLCP
Genistein	25.0	Blocks tyrosine kinases, prevents branching
Jasplakinolide	0.07	Promotes linear and branched growth of actin fibers
Latrunculin A	1.0	Binds to G-actin, net depolymerization
ML-7	30.0	MLCK inhibitor
Phallacidin	1.0	Phalloidin analog, actin cross-linking
Phalloidin oleate	1.0	Phalloidin analog, actin cross-linking

5-HT, serotonin; DBcAMP, dibutyryl adenosine 3′,5′-cyclic monophosphate; MLCK, myosin light-chain kinase; $[Ca^{2+}]_i$, intracellular Ca^{2+} concentration; MLCP, myosin light-chain phosphatase; G-actin, monomeric actin; ML-7, 1-(5-iodonaphthalene-1-sulfonyl)-1H-hexahydro-1,4-diazepine.

Cell preparation. When ASM cells (*passages 3–8*) were confluent, they were serum deprived for 24 h. To create ITS medium, we added sodium selenite (6.7 mg/ml), transferrin (5.5 mg/ml), and insulin (10 mg/ml) to serum-free DMEM-Ham's F-12 medium. Cells were released from the flasks using trypsin and then plated at 30,000 cells/well. Plastic wells (96-well plate; Corning, Corning, NY) were previously coated with collagen at 500 ng/cm^2. Cells were allowed to adhere to the matrix overnight before use.

Bead preparation. Ferrimagnetic microbeads (Fe_3O_4, 4.5-μm diameter) were produced in our laboratory at the Harvard School of Public Health (15, 29). Beads were coated for at least 24 h with RGD peptide (200 μg/mg beads) in carbonate buffer (pH 9.4). On the day of the experiments, beads were added to FBS-free medium with 1% BSA. The presence of BSA permitted the specific binding of the beads to the integrin receptors on the surface of the cells.

Optical magnetic twisting cytometry. Cell mechanical properties were measured using magnetic twisting cytometry with optical detection of bead motion (15, 42). Serum-deprived cells were plated on collagen-coated wells, incubated with ferrimagnetic beads (20 min), and then washed with medium to remove unbound beads. Wells were held on the stage of an inverted microscope. The apparatus contained two sets of coils and a temperature controller. All experiments were performed at 37°C. The beads were magnetized horizontally so that their magnetic moments were aligned in the plane of the plate's surface. A second magnetic field, the twisting field, was applied vertically. This second field caused the beads to rotate and translate, tending to orient their magnetic moment with the direction of applied field. As the beads twisted, they exerted a stress on the adhesion receptors, the focal adhesion complex, and other CSK structures that had formed around the beads (7, 15, 42). The stress was transmitted to the cell and its underlying structures, which, because of their own elastic and frictional properties, impeded the movement of the bead. A frequency scan was performed by increasing frequency and then rescanned with decreasing frequency to check for history dependence. The frequencies imposed were 0.01, 0.03, 0.1, 0.3, 0.75, 4.2, 10, 30, 100, 300, and 1,000 Hz.

Experimental protocols. After ferrimagnetic beads were added and wells were washed, cells were ready for investigation. Cells were tested at the start of each experimental day for their sensitivity to the drugs. These wells were used for one run and then discarded. For frequency scans, each well was run twice: once in baseline conditions and once after the addition of drug. In this way, each well served as its own control. For each well, the first scan was performed, and then the well was removed from the microscope and set aside while the chosen drug was added. The well was then placed back onto the microscope stage, remagnetized, and the second frequency scan was performed. Only one drug was tested in each well. For a negative

control (sham), ITS medium was added. Each drug was studied in multiple wells on multiple days. Table 2 shows the number of beads from which data were collected for each drug.

Measurement of mechanical properties. The twisting field was adjusted for each well and treatment so that oscillatory bead displacement was ~100 nm. Displacements of each bead were recorded using a charge-coupled device camera. Bead position was analyzed online using an intensity-weighted center-of-mass algorithm that yielded an accuracy of <5 nm. We eliminated beads from subsequent data analysis when their movement in the original magnetization direction was smaller than their movement perpendicular to the magnetization direction. The mechanical properties of the cell were calculated from the imposed torque and the measured bead motions. At each frequency, the complex cell stiffness g^* was defined as the complex ratio of the specific torque to bead displacement (Pa/nm) as described below. g^* was measured for each bead; the real part of g^* (the elastic or stiffness modulus) is denoted g' and the imaginary part of g^* (the loss modulus) is denoted g''. For each well, the median values at each frequency of g' and g'' were calculated. These medians were then grouped by drug and averaged. To control for day-to-day variability, data for each day were corrected to the baseline values of all wells on all days; this correction did not affect the frequency dependence. For those frequencies measured twice, the two measurements were combined using the complex geometric mean, but our results remained the same if we used arithmetic means instead. In Figs. 1–3, data points represent the median value of g' or g'' for each treatment at each given testing frequency. The geometric means of g' and g'' at each frequency under each condition were used for further analysis.

Data analysis. Our data were described by the structural damping law with an additive Newtonian viscosity term,

$$g^*(\omega) = g' + ig'' = (i\omega)^{x-1}G\Gamma(2-x) + i\omega\mu \qquad (1)$$

where $i = \sqrt{-1}$, $x - 1$ is the power law exponent, G is a scale factor, μ is the Newtonian viscosity, and the radian frequency ω is $2\pi f$ (14, 15). The Γ function $\Gamma(2 - x)$ appears in the Fourier domain assuming that the stress relaxation function is t^{1-x} in the time domain (25). g' (the real part of the complex modulus) increases with frequency according to the power law exponent, $x - 1$. g'' (the imaginary part of the modulus) includes a component that also increases as a power law with the same exponent. According to *Eq. 1*, the parameter x is an index along the spectrum from solidlike ($x = 1$) to fluidlike ($x = 2$) behavior (5, 14, 15, 38, 39). In the limit in which x approaches 1, the behavior approaches that of a Hookean elastic solid, while in the limit in which x approaches 2, the behavior approaches that of a Newtonian viscous fluid. Thus the structural damping equation describes a relationship between changes of the exponent in the power law and the transition from solidlike to fluidlike behavior.

The theory of soft glass rheology predicts material behavior according to the structural damping equation (*Eq. 1*). In that theory, x is associated with athermal mechanisms of agitation in the microenvironment and plays a role akin to a temperature and for that reason has been called the effective temperature (5, 15, 38). Moreover, the parameter x and the structure-damping coefficient (loss tangent) η are directly related to one another; when η is small compared with unity, $\eta = 1 - x$, but more generally, $\eta \tan[(x - 1)\pi/2]$.

g' and g'' have units of Pa/nm. These values can be converted into traditional elastic and loss moduli (in Pa units) through multiplication by a geometric scale factor α that depends on the shape and thickness of the cell and the degree of the bead embedding. Finite element analysis of cell deformation previously published by Mijailovich et al. (28) fixed α at roughly 6.8 μm. This finding assumed a homogeneous and isotropic elastic area surrounding the site of bead embedding, a 5-μm cell height, and 10% embedding of the bead into the cell.

Statistical analysis. We compared three models, all based on the structural damping equation. These models differed only with regard to which parameters were held to be common among the conditions and which were allowed to differ.

Model I is fully unconstrained. There were separate G, x, and μ values for each drug. Taken together, g' vs. frequency f, all data across separate drug interventions appeared to converge at a common intersection point, which we denote g_0,f_0. Because of the Γ function in *Eq. 1*, there is not one common intersection, but all curves do cross in the same vicinity. Regarding Models II and III (see below), the choice of model influenced the position of the apparent common intersection point, (g_0,f_0). In Model II, all relationships were forced to have a common (g_0,f_0) parameter pair that was determined by the fit. This finding corresponds to the empirical observation in some sets of data that the stiffness plots (g') all seemed to intersect at one point (g_0,f_0). In Model III, the further constraint was imposed that all data had the same viscosity (μ), which might reflect the background cytosol through which cytoskeletal components move.

Fits to the data were obtained by minimizing the sum of the squared magnitudes of the difference between the logarithm of the complex data and the logarithm of the complex prediction from *Eq. 1*. Logarithms were used both because a power law becomes linear in log space, and because the observed variability is approximately log-normal and becomes normal in log space (15, 16). Fits to the data were done using the R statistical analysis package version 1.6.2 (The Comprehensive R Archive Network, http://cran.r-project.org/). This procedure was repeated for all three models.

ANOVA was performed to evaluate the parameters of the fits and to compare these models using a reduction-in-variance F-test. If the observed P value was <0.05, we concluded that there were significant differences between models.

Methodological limitations. Methodological limitations of the bead-twisting approach for the assessment of cell rheology have been described in detail in a recent publication (32).

Table 2. *Stiffness, slope, and viscosity of beads for all treatments*

Treatment	No. of Beads Measured per Treatment	g' at 0.75 Hz, Pa/nm	x	$\mu \times 10^{-5}$, Pa*s/nm
Baseline	6,630	0.059±0.171	1.20±0.0066	3.81±0.33
Sham	1,196	0.065±0.005	1.20±0.0066	4.35±0.37
Latrunculin A	435	0.015±0.002	1.27±0.0075	3.51±0.21
Cytochalasin D	756	0.034±0.006	1.21±0.007	3.80±0.27
Phallacidin	489	0.069±0.015	1.19±0.0065	4.14±0.37
Phalloidin oleate	619	0.053±0.005	1.21±0.0066	3.74±0.32
Jasplakinolide	747	0.099±0.011	1.20±0.0066	7.57±0.56
Genistein	834	0.056±0.005	1.22±0.0068	6.26±0.42
5-HT	977	0.111±0.011	1.18±0.0066	7.09±0.56
DBcAMP	1,033	0.023±0.002	1.26±0.0074	5.06±0.29
ML-7	603	0.038±0.014	1.22±0.007	4.79±0.32

Stiffness g' is the geometric mean ± SE, x is slope, and μ is mean viscosity ± SE.

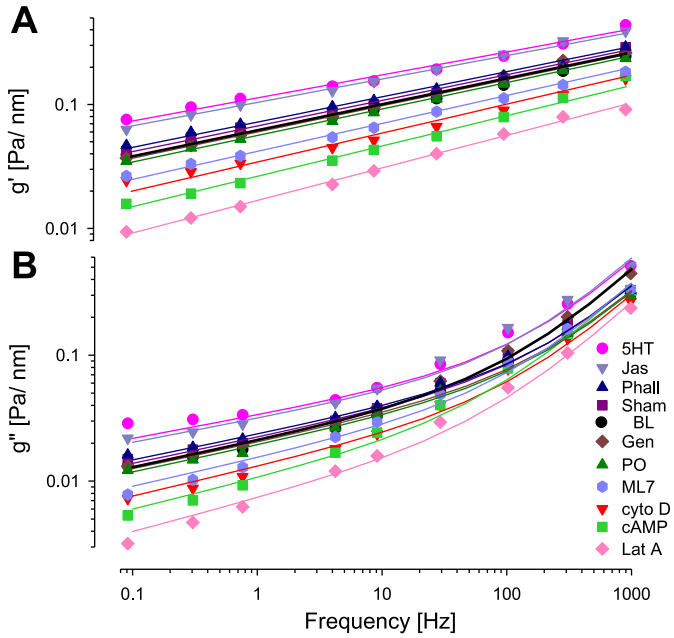

Fig. 1. Line graphs showing stiffness g' (*A*) and loss modulus g'' (*B*) vs. frequency. The solid lines are the fits of *Eq. 1* $\{g^*[\omega = g' + ig'' = (i\omega)^{x-1}\, G]\,\Gamma(2 - x) + i\omega\mu\}$ using Model II. g' and g'' are expressed in Pa/nm; these values can be converted into traditional elastic and loss moduli (in Pa units) through multiplication by a geometric scale factor α, which depends on the shape and thickness of the cell and the degree of the bead embedding. Finite element analysis of cell deformation previously published by Mijailovich et al. (28) fixes α at ~6.8 μm. BL, baseline (●); Lat, latrunculin A, Cyto, cytochalasin D, PO, phalloidin oleate; Phall, phallacidin; Gen, genistein, Jas, jasplakinolide.

RESULTS

Stiffness. Baseline measurements (Fig. 1*A*) showed a weak increase in stiffness with increasing frequency that was well fitted by power law behavior. For treatments in which the actin network was disrupted, such as with latrunculin A, g' fell but the power law exponent $x - 1$ increased. When the cells were activated by 5-HT or when actin was polymerized, as with jasplakinolide, g' increased but the power law exponent decreased. At a given frequency, differences in stiffness from the largest values to the smallest approached an order of magnitude. Despite these large variations, in every case, g' followed the same kind of weak power law behavior.

Friction. The baseline measurement friction data (Fig. 1*B*) also exhibited weak frequency dependence. g'' followed the same weak power law behavior as did g' at lower frequencies, but at larger frequencies it exhibited a stronger frequency dependence approaching a power law exponent of 1, which is characteristic of Newtonian viscosity. As with g', when the actin network was disrupted, g'' fell and the exponent of the low-frequency power law increased. Again, as with g', when the cells were activated or actin was polymerized, g'' increased and the exponent of the low-frequency power law component decreased.

Structural damping equation. All data were well described by *Eq. 1* (fits denoted by solid lines in Fig. 1, Model II). When we fit the structural damping equation to the complex moduli for each of the treatment conditions, we obtained a parameter set for x, g_0, f_0, and μ. We evaluated how well the structural damping equation accounted for the data when either all parameters were free across drug treatments (Model I), when (g_0, f_0) was constrained to be the same for all drug treatments (Model II), or when g_0, f_0, and μ were constrained to be the same for all drug treatments (Model III). The residual variances of the fits of Models I and II were significantly different from each other ($P = 0.0016$). Thus ANOVA rejected Model II compared with Model I. However, both correlation coefficients were high: R^2 values were 0.9933 and 0.9926, respectively. We thus argue that Model II, with fewer parameters, captured the essence of the data.

A constrained (common) viscous term over treatments (Model III) resulted in a fit with $R^2 = 0.9886$, which was statistically poorer than Model I or Model II ($P = 1.7 \times 10^{-14}$, Model II vs. Model III). This finding would indicate that the Newtonian viscosity term changed in response to drug treatment. On the other hand, the changes in viscosity were small compared with drug-induced changes of g' and g'' at lower frequencies. Thus, for our purposes μ could also be regarded as being approximately invariant with drug treatment. Values for g', μ (both from Model II), and x (from Model I) are listed in Table 2.

Scaling data onto master curves. Because power law responses are straight lines on log-log graphs, each of the relationships of g' vs. f could be defined by one point (which we chose arbitrarily as the value measured at 0.75 Hz) and one slope ($x - 1$). To compare responses between drug interventions, we normalized the data using the approach described previously by Fabry et al. (15). We used the common intersection stiffness g_0 as a stiffness scale and then defined normalized cell stiffness, G_{norm}, as $g'_{0.75\ Hz}/g_0$. To scale the cell's frictional properties, we used the ratio g''/g' (hysteresivity, or loss tangent, η) at 0.75 Hz. We used x from the fit of the structural damping equation using Model I and then plotted G_{norm} vs. x and η vs. x (Fig. 2), for which Model I was used because it is the least constrained. When the stiffness and friction data were normalized in this way, they collapsed onto two master relationships. Drugs that increased x caused the normalized stiffness to decrease and the hysteresivity to increase. These relationships fell close to the predictions from the structural damping equation (Fig. 2).

Common intersection at high frequency. Differences in stiffness among various experimental conditions became progressively smaller as the frequency increased (Figs. 1*A* and Fig. 3). When the family of lines shown in Fig. 1*A* was extrapolated, the difference in stiffness approximately vanished at some high frequency f_0 (Fig. 3). In Fig. 3, the red ellipse indicates the 95% confidence interval for this intersection point, and similar confidence intervals obtained in previous reports using different cell populations are shown for comparison. Because of the small slopes, the small differences in slopes, and the fact that the approximate intersection fell well beyond the experimental range, the intersection frequency f_0 was not well determined. In no case was f_0 lower than the MHz range, however, and more typically it was in the GHz range (Fig. 3).

DISCUSSION

The data presented herein confirm and substantially extend the original findings of Fabry et al. (14) showing that weak power law responses seem to be a pervasive feature of cytoskeletal rheology (Fig. 1). In addition, all data collapsed onto

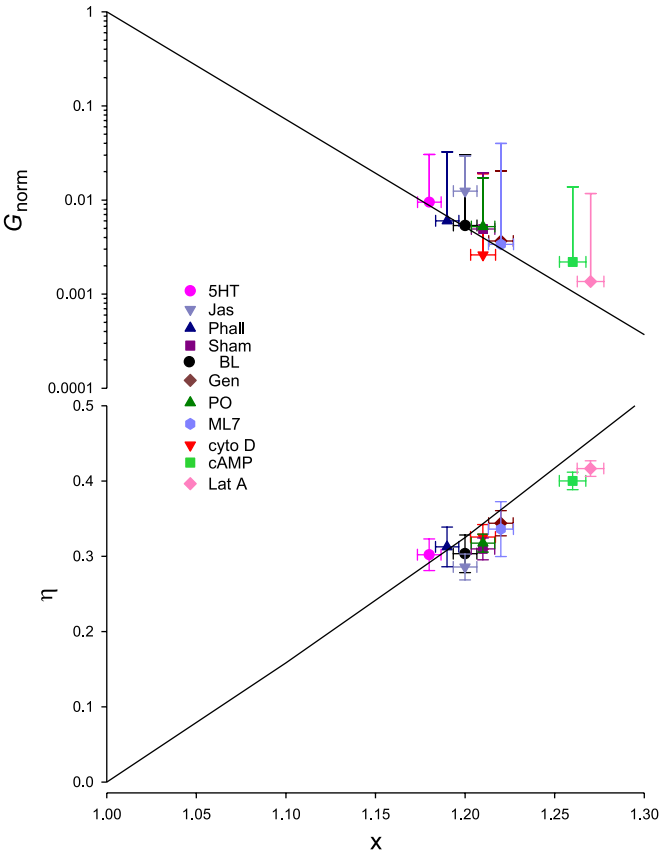

Fig. 2. The cytoskeleton (CSK) sits along a continuous spectrum of solidlike vs. fluidlike states in which the limit $x = 1$ corresponds to a perfect Hookean elastic solid and the limit $x = 2$ corresponds to a perfect Newtonian viscous fluid. *A*: master curve of normalized stiffness $G_{norm} = g'$ (0.75 Hz)/g_0. *B*: master curve of hysteresis η (0.75 Hz) vs. x. Solid lines are predictions from *Equation 1*: $\ln G_{norm} = (x - 1) \ln(\omega\omega)$ (*A*) and $\eta = \tan[(x - 1)\pi/2]$ (*B*). g_0 and f_0 are determined from Model II and x is determined from Model I. Horizontal error bars show SE. Vertical error bars show SD, which were used because SE values were too small to be visible.

two unifying master relationships, one depicting elasticity and the other depicting friction. Together with previous reports (1, 8, 14, 15, 17, 25, 32, 37), these new data demonstrate that across a wide range of cell types, probing technologies, molecular couplings, time scales, and manipulations, when the mechanical properties of the cell change, they do so along a special trajectory (Fig. 2). That trajectory is controlled solely by the value of x, and the specific intervention seems not to matter. What did matter was the ability the specific intervention to modulate x, where x in turn set the dynamics.

We addressed methodological limitations in MATERIALS AND METHODS and note that the panel of interventions used in this study was wide and the results obtained were mutually consistent, and as such, the chance of misinterpretation on the basis of the nonspecific effects of any one agent was small. Each intervention served as a positive control for the others, and stiffness and frictional moduli showed large changes in the expected directions.

Glassy dynamics. Fabry and colleagues (14, 15) noted that the power law behavior observed in cells is strongly analogous to the behavior observed in soft glassy materials such as foams, pastes, and colloids, and they speculated that the parameter x defined in *Eq. 1* might be associated with the effective temperature that had been postulated by Sollich and colleagues (38, 39) to control the dynamics of such systems. In a recent publication, this analogy was supported by a broader range of biophysical observations (5, 36).

This analogy suggests the following physical picture. Cytoskeletal dynamics in the ASM are proposed to fit within the framework of the trapping of a CSK structural protein or protein complex in a deep energy well, i.e., a well so deep that thermal collisions are insufficient to drive the protein or protein complex out of the well (5, 13–15, 21, 36). If thermal forces are insufficient, then hopping out of the well is imagined to be driven by nonthermal energies that are much larger than k_BT (where k_B is Boltzmann's constant) but can be expressed nonetheless as an effective temperature of the CSK matrix.

Formally, the term "temperature" means molecular motion and carries with it the connotation of molecular collisions and resulting agitation caused by ongoing molecular bombardments of thermal origin. Herein the term "effective temperature" is meant to carry with it a similar connotation of molecular agitation but caused by processes that may be of nonthermal origin. A protein conformational change fueled by hydrolysis of ATP, for example, releases energy that is 25-fold greater than thermal energy (22) and does so at the rate of $>1 \times 10^4$ events·s^{-1}·μm^{-3} of cytoplasm (21). Accordingly, such events would have the potential to jostle a neighboring structure rather substantially and dislodge it from a relatively deep energy well.

Physical interactions that lead to trapping might include molecular crowding, hydrogen bonding, or weak cross linking (10–12, 34, 41). With regard to molecular crowding, the volume fraction of macromolecules within the cell approaches the maximum packing fraction that is possible, with the mean distance between macromolecules being only 2 nm (31). The molecular space within a cell is so crowded, in fact, that crowding can change binding affinities between specific proteins by orders of magnitude (9, 10, 12, 20). If trapping is due to nonspecific mechanisms such as molecular crowding or hydrogen bonding, then the specific properties of cross-linking molecules might be of only secondary importance. One rubric illustrating this possibility is shown in Fig. 4, in which the effective temperature x is shown as the central factor controlling CSK dynamics. If trapping has its origins in the cross

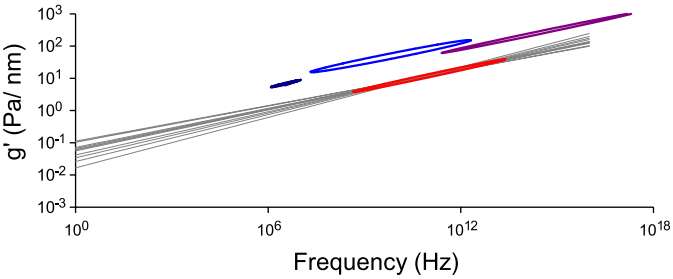

Fig. 3. Shaded lines represent the extrapolation of the fitted data to the intersection point using Model II. The 95% confidence interval regions for the common fixed points (g_0,f_0) are shown. The fit of the rat airway smooth muscle (ASM) data from the current study is shown in red ($f_0 = 1.1 \times 10^{11}$ Hz). For comparison, three human ASM intervals are displayed from previous publications by Fabry et al. (15) ($f_0 = 3.4 \times 10^6$ Hz) (dark blue), Puig-de-Morales et al. (32) ($f_0 = 6.5 \times 10^9$ Hz) (blue), and Lenormand et al. (25) ($f_0 = 7.8 \times 10^{13}$ Hz) (purple).

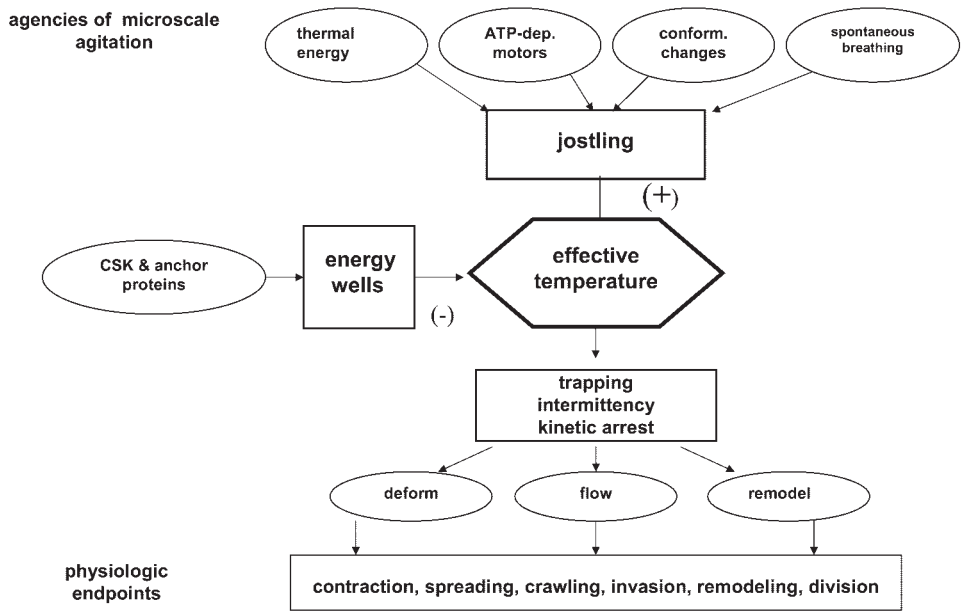

Fig. 4. Data in Figs. 1 and 2 suggest that specific molecular interactions might influence integrative dynamics only to the extent that they modify the effective temperature. In this diagram, one possible explanation is shown. *Jostling*: in addition to ordinary thermal agitation (k_BT) and the tidal action of spontaneous breathing, other agencies contributing to the intracellular molecular agitation potentially include ruffling, vesicle transport, and any local motions caused by proteins that undergo cyclic conformational changes, including molecular motors, ribosomes, and G proteins. These ongoing conformational changes jostle nearby cages by mechanisms that are ATP dependent. Associated local motions are quite large, in the 1- to 10-nm range, which are comparable to molecular dimensions and molecular spacing (22). The mechanical energy released is also quite large, about half of the chemical energy derived from hydrolysis of the γ-phosphate bond of ATP, or ~10 k_BT/event (22). For 1 μm^3 of cytoplasm of a typical cell, these events occur at a rate of $>1 \times 10^4$/s (21). *Energy wells*: energy wells that constrain motion are imagined to deepen with the buildup of weak bonds and geometrical constraints associated with CSK polymerization and cross linking. Deepening of such wells would be reflected in a falling noise temperature. *Trapping, intermittency, kinetic arrest*: this hypothesis rests on only conservative assumptions, namely, that the CSK comprises elements aggregated with one another via interactions that are numerous, weak, and complex. As a result, these interactions are metastable, and associated stochastic hopping events lead to lattice disorder (5, 13, 15, 21). The physiological end point is that an attractive feature of this hypothesis is its explanatory power. It attempts to explain with a single, unifying mechanism three aspects of cytoskeletal function that have been investigated previously as largely distinct and independent events: deformability, flow, and remodeling.

linking of CSK filaments, however, then the density and the specific type of cross links and CSK filaments, as well as the dynamics of their specific interactions, might be crucial (19). Many of the cytoskeletal modulations that we have used to date alter both macromolecular packing and the dynamics of cross-linked filament networks (27), and thus they cannot determine which of the two interactions might play a dominant role. Regardless of the particular interaction, trapping is hypothesized to arise as a result of the insufficiency of thermal energy to drive CSK structural rearrangements (41). The collapse of all data onto master curves reported herein suggests that specific molecular interactions influence CSK stiffness and friction, but only to the extent that these interactions can modify the effective temperature.

Intersection at high frequency. The existence of a common intersection at high frequency, f_0, remains an empirical finding with no known mechanistic basis (Fig. 3). Nonetheless, it is highly consequential, because it accounts for the fact that all data can be described by only one parameter, x (Fig. 1), and therefore collapse onto unifying master relationships (Fig. 2). All stiffness spectra were observed to pivot about one fixed point (g_0,f_0), and for this reason, each stiffness spectrum was set solely by x (Figs. 1, 3).

The mechanism that accounts for the intersection remains a matter of speculation. Protein-protein interactions of various kinds exhibit molecular relaxation time scales that span 15 orders of magnitude (4), and this profound heterogeneity might plausibly account for the wide range of relaxation times implied by Fig. 1. Heterogeneity by itself cannot explain why the distribution of relaxation times follows the special form of a weak power law, however, and neither can it explain the special relationship among the power law exponents implied by the approximate intersection at f_0 and the collapse of all data as demonstrated in Fig. 2.

That such a simple phenomenological framework can describe such a complex system is counterintuitive. Factors that are common to every case, however, are the presence of water and molecular crowding. Surrounding hydrating shells strongly influence protein-protein dynamics, and in turn the presence of a nearby protein surfaces strongly influences water dynamics. Water becomes ordered in the vicinity of some macromolecules, and within the cell the average distance between macromolecules is only 2 nm, or roughly 10 water molecules across (31). Suzuki and co-workers (18, 23, 40) have suggested that water molecules within the cell interact with protein surfaces in broad categories. Bulk water forms a hydrogen-bonding network but remains relatively mobile. Water molecules that interact with protein surfaces are typically less mobile than water molecules in bulk water because the protein reinforces the hydrogen-bonding network of neighboring water molecules. Water that is strongly bound in deep clefts is the least mobile. Interestingly, water in the vicinity of F-actin is hypermobile, perhaps because actin induces breaking in the water network. Suzuki et al. (40) pointed out that the volume

fraction of hypermobile water is as great as 80% of the molecular volume of G-actin.

The rotational mobility of water has been measured using microwave dielectric spectroscopy, which shows that the relaxation frequency of hypermobile water is ~40 GHz, that of bulk water is 17 GHz, and that of hydrating water near globular proteins is 4–8 GHz or less (18, 23, 40). This range of relaxation frequencies coincides with the range of estimates for the intersection frequency f_0 shown in Fig. 3. We speculate that if the cell were perturbed mechanically at a frequency corresponding to the rotational relaxation frequency of water, the water network might dominate the mechanical response of the system and differences in stiffness with various CSK interventions might vanish. Nonetheless, it remains unclear whether molecular crowding and resulting water-protein interactions might help to account for the simplicity and nonspecificity of the findings reported herein or the existence of the intersection.

In summary, we have discovered general physical laws that appear to govern the mechanical behavior of the cytoskeleton (5, 14, 15, 25, 32, 36), and in the present study, we have extended the generality of those behaviors. These laws bring together into one physical picture cytoskeletal elasticity, friction, and remodeling and show that that the cell is a strange intermediate form of matter that is neither solid nor fluid but retains features of both; classical theories of viscoelasticity, equilibrium systems, and the Stokes-Einstein relationship fail to account for these observations (5). Moreover, these observations establish that the cell possesses a temperature-like property that determines where the CSK sits along a continuous spectrum of solidlike vs. fluidlike states (Fig. 2).

Major unsolved problems in science were recently highlighted (24), and among those identified were the structure of water, protein-protein interactions, the dynamics of nonequilibrium systems, and the nature of the glassy state. The mechanics of the CSK would appear to find itself at a convergence of these unsolved problems, and this convergence represents both a challenge and an opportunity. Although the mechanism of action remains uncertain, the unifying phenomenological framework reported herein is striking. Even in the absence of a mechanism, it is possible that this framework may provide a simplified way to think about bronchospasm, vasospasm, wound repair, embryonic development, cell invasion, and any other cellular processes that have important mechanical components.

ACKNOWLEDGMENTS

We thank Marc Molenat for bead production and Paulo Silveira, Guillaume Lenormand, and Marina Puig-de-Morales for their comments on and critical reading of the manuscript.

GRANTS

This study was supported by National Heart, Lung, and Blood Institute HL-33009, HL-65960, HL-07118, and HL-59682.

REFERENCES

1. **Alcaraz J, Buscemi L, Grabulosa M, Trepat X, Fabry B, Farré R, and Navajas D.** Microrheology of human lung epithelial cells measured by atomic force microscopy. *Biophys J* 84: 2071–2079, 2003.
2. **An SS, Laudadio RE, Lai J, Rogers RA, and Fredberg JJ.** Stiffness changes in cultured airway smooth muscle cells. *Am J Physiol Cell Physiol* 283: C792–C801, 2002.
3. **Balland M, Richert A, and Gallet F.** The dissipative contribution of myosin II in the cytoskeleton dynamics of myoblasts. *Eur Biophys J* 34: 255–261, 2005.
4. **Bao G and Suresh S.** Cell and molecular mechanics of biological materials. *Nat Mater* 2: 715–725, 2003.
5. **Bursac P, Lenormand G, Fabry B, Oliver M, Weitz DA, Viasnoff V, Butler JP, and Fredberg JJ.** Cytoskeletal remodelling and slow dynamics in the living cell. *Nat Mater* 4: 557–571, 2005.
6. **Chopra LC, Hucks D, Twort CH, and Ward JP.** Effects of protein tyrosine kinase inhibitors on contractility of isolated bronchioles of the rat. *Am J Respir Cell Mol Biol* 16: 372–378, 1997.
7. **Deng L, Fairbank NJ, Fabry B, Smith PG, and Maksym GN.** Localized mechanical stress induces time-dependent actin cytoskeletal remodeling and stiffening in cultured airway smooth muscle cells. *Am J Physiol Cell Physiol* 287: C440–C448, 2004.
8. **Desprat N, Richert A, Simeon J, and Asnacios A.** Creep function of a single living cell. *Biophys J* 88: 2224–2233, 2005.
9. **Dobson CM.** Chemical space and biology. *Nature* 432: 824–828, 2004.
10. **Ellis RJ.** Macromolecular crowding: an important but neglected aspect of the intracellular environment. *Curr Opin Struct Biol* 11: 114–119, 2001.
11. **Ellis RJ.** Macromolecular crowding: obvious but underappreciated. *Trends Biochem Sci* 26: 597–604, 2001.
12. **Ellis RJ and Minton AP.** Cell biology: join the crowd. *Nature* 425: 27–28, 2003.
13. **Fabry B and Fredberg JJ.** Remodeling of the airway smooth muscle cell: are we built of glass? *Respir Physiol Neurobiol* 137: 109–124, 2003.
14. **Fabry B, Maksym GN, Butler JP, Glogauer M, Navajas D, and Fredberg JJ.** Scaling the microrheology of living cells. *Phys Rev Lett* 87: 148102, 2001.
15. **Fabry B, Maksym GN, Butler JP, Glogauer M, Navajas D, Taback NA, Millet EJ, and Fredberg JJ.** Time scale and other invariants of integrative mechanical behavior in living cells. *Phys Rev E Stat Nonlin Soft Matter Phys* 68: 041914, 2003.
16. **Fabry B, Maksym GN, Hubmayr RD, Butler JP, and Fredberg JJ.** Implications of heterogeneous bead behavior on cell mechanical properties measured with magnetic twisting cytometry. *J Magnetism Magn Mater* 194: 120–125, 1999.
17. **Fabry B, Maksym GN, Shore SA, Moore PE, Panettieri RA Jr, Butler JP, and Fredberg JJ.** Signal transduction in smooth muscle: Selected contribution: Time course and heterogeneity of contractile responses in cultured human airway smooth muscle cells. *J Appl Physiol* 91: 986–994, 2001.
18. **Fuller N and Rand RP.** Water in actin polymerization. *Biophys J* 76: 3261–3266, 1999.
19. **Gardel ML, Shin JH, MacKintosh FC, Mahadevan L, Matsudaira P, and Weitz DA.** Elastic behavior of cross-linked and bundled actin networks. *Science* 304: 1301–1305, 2004.
20. **Goodsell D.** Biomolecules and nanotechnology. *Am Sci* 88: 230–237, 2000.
21. **Gunst SJ and Fredberg JJ.** The first three minutes: smooth muscle contraction, cytoskeletal events, and soft glasses. *J Appl Physiol* 95: 413–425, 2003.
22. **Howard J.** *Mechanics of Motor Proteins and the Cytoskeleton*. Sunderland, MA: Sinauer, 2001.
23. **Kabir SR, Yokoyama K, Mihashi K, Kodama T, and Suzuki M.** Hyper-mobile water is induced around actin filaments. *Biophys J* 85: 3154–3161, 2003.
24. **Kennedy D and Norman C.** What don't we know? *Science* 309: 75, 2005. doi:10.1126/science.309.5731.75.
25. **Lenormand G, Millet E, Fabry B, Butler JP, and Fredberg JJ.** Linearity and time-scale invariance of the creep function in living cells. *J Roy Soc Interface* 1: 91–97, 2004. doi:10.1098/rsif.2004.0010.
26. **Mack CP, Somlyo AV, Hautmann M, Somlyo AP, and Owens GK.** Smooth muscle differentiation marker gene expression is regulated by RhoA-mediated actin polymerization. *J Biol Chem* 276: 341–347, 2001.
27. **Mehta D and Gunst SJ.** Actin polymerization stimulated by contractile activation regulates force development in canine tracheal smooth muscle. *J Physiol* 519: 829–840, 1999.
28. **Mijailovich SM, Kojic M, Zivkovic M, Fabry B, and Fredberg JJ.** A finite element model of cell deformation during magnetic bead twisting. *J Appl Physiol* 93: 1429–1436, 2002.
29. **Möller W, Scheuch G, Sommerer K, and Heyder J.** Preparation of spherical monodisperse ferrimagnetic iron-oxide microparticles between 1 and 5 μm diameter. *J Magnetism Magn Mater* 225: 8–16, 2001.

30. **Park JK, Lee SO, Kim YG, Kim SH, Koh GY, and Cho KW.** Role of rho-kinase activity in angiotensin II-induced contraction of rabbit clitoral cavernosum smooth muscle. *Int J Impot Res* 14: 472–477, 2002.
31. **Pollack GH.** *Cells, Gels and the Engines of Life: A New, Unifying Approach to Cell Function*. Seattle, WA: Ebner & Sons, 2001.
32. **Puig-de-Morales M, Millet E, Fabry B, Navajas D, Wang N, Butler JP, and Fredberg JJ.** Cytoskeletal mechanics in adherent human airway smooth muscle cells: probe specificity and scaling of protein-protein dynamics. *Am J Physiol Cell Physiol* 287: C643–C654, 2004.
33. **Sawitzky H, Hanfstingl U, and Faulstich H.** Growth inhibition and changes in morphology and actin distribution in *Acetabularia acetabulum* by phalloidin and phalloidin derivatives. *Protoplasma* 220: 209–218, 2003.
34. **Segrè PN, Prasad V, Schofield AB, and Weitz DA.** Glasslike kinetic arrest at the colloidal-gelation transition. *Phys Rev Lett* 86: 6042–6045, 2001.
35. **Selig WM, Bloomquist MA, Cohen ML, and Fleisch JH.** Serotonin-induced pulmonary responses in the perfused guinea pig lung: evidence for 5HT2 receptor-mediated pulmonary vascular and airway smooth muscle constriction. *Pulm Pharmacol* 1: 93–99, 1988.
36. **Seow CY.** Biophysics: fashionable cells. *Nature* 435: 1172–1173, 2005.
37. **Smith BA, Tolloczko B, Martin JG, and Grütter P.** Probing the viscoelastic behavior of cultured airway smooth muscle cells with atomic force microscopy: stiffening induced by contractile agonist. *Biophys J* 88: 2994–3007, 2005.
38. **Sollich P.** Rheological constitutive equation for a model of soft glassy materials. *Phys Rev E Stat Nonlin Soft Matter Phys* 58: 738–759, 1998.
39. **Sollich P, Lequeux F, Hébraud P, and Cates ME.** Rheology of soft glassy materials. *Phys Rev Lett* 78: 2020–2023, 1997.
40. **Suzuki M, Kabir SR, Siddique MSP, Nazia US, Miyazaki T, and Kodama T.** Myosin-induced volume increase of the hyper-mobile water surrounding actin filaments. *Biochem Biophys Res Commun* 322: 340–346, 2004.
41. **Trappe V, Prasad V, Cipelletti L, Segre PN, and Weitz DA.** Jamming phase diagram for attractive particles. *Nature* 411: 772–775, 2001.
42. **Wang N, Butler JP, and Ingber DE.** Mechanotransduction across the cell surface and through the cytoskeleton. *Science* 260: 1124–1127, 1993.
43. **Warbanow W and Will-Shahab L.** Decreased contractile response after exposure of the rat aorta to DbcAMP or IBMX. *Biomed Biochim Acta* 46, *Suppl*: S477–S481, 1987.